Electronic supplementary information

Enhanced Water Purification via Redox Interfaces Created by an Atomic Layer Deposition Strategy

Liming Huang[a,†], Tingting Yan[a,†], Alaa El Din Mahmoud[b], Shuangxi Li[a], Jianping Zhang[a], Liyi Shi[a], and Dengsong Zhang[a,*]

[a] Department of Chemistry, State Key Laboratory of Advanced Special Steel, International Joint Laboratory of Catalytic Chemistry, College of Sciences, Shanghai University, Shanghai, 200444, China.

[b] Environmental Sciences Department, Faculty of Science, Alexandria University, Alexandria, 21511, Egypt.

[†] These authors contributed equally for this work.

*E-mail: dszhang@shu.edu.cn

Table of Contents

■ Experimental Section

Materials.

Graphene (rGO) was supplied by Graphene-king Company. Titanium tetrachloride ($TiCl_4$), dopamine hydrochloride ($C_8H_{11}NO_2 \cdot HCl$) and tetraethyl orthosilicate ($Si(OC_2H_5)_4$) were provided by Aladdin. Ammonia solution ($NH_3 \cdot H_2O$), ethanol (C_2H_6O) and sodium hydroxide (NaOH) were provided by Sinopharm Chemical Reagent Co. Ltd. in China. All the chemicals were used without further purification.

Synthesis of silicon dioxide microspheres.

14 mL ammonia solution was dispersed into 300 mL ethanol and 40 mL deionized water. Then the mixture solution was taken in the water bath heating at 30 ℃ and stirring for 30 min. After, 24 mL tetraethyl orthosilicate was added quickly in the solution through ultrasonication for 30 min. After then, the solution was heated during 30 ℃ and stirred for 30 min again in the water bath. After that, the aqueous suspension of mono-dispersed silicon dioxide microspheres were obtained by centrifugation while washing with ethyl alcohol and deionized water several times.

Synthesis of titanium dioxide/porous carbon (CTO-PC) prepared by an impregnation method.

At the first, 80 mg PC was dispersed into 200 mL absolute ethyl alcohol and 50 mL water deionized water by continuous ultrasonication and stirring. Then 20 mL $TiCl_4$ solution was added drop by drop under the mixed solution. Afterward the solution was stirring at room temperature for 12 h. The precipitate was separated by centrifugation and washed through ethanol and deionized water. Subsequently, the precipitate was

dried overnight at 80 ℃. The CTO-PC was acquired by calcined at 150 ℃ for 5 h with a ramping rate of 2 ℃/min under flowing N_2.

■ Characterization and Test

The morphology and microstructure of the samples were obtained by transmission electron microscopy (TEM, JEOL, JEM-200CX), scanning electron microscopy (SEM, JEOL, JEM-700F), high-resolution transmission electron microscopy (HTEM, JEOL, JEM-2010F) and Micromeritics ASAP 2010 analyzer, X-ray diffractometer (XRD, Rigaku D/MAX-RB, Cu Kα, 40 kV, 20mA), X-ray photoelectron spectroscopy (XPS, Perkin-Elmer PHI 5000C, Mg Kα, 1253.6 eV), A drop shape analysis system (Kruss, DSA100), respectively.

The material resistivity of different samples was measured by a four-point probe (Model 280SI). The dates based on at least five independent measurements under different positions in the prepared electrode surface. Besides, the electrochemical behaviors of sample were observed by electrochemical impedance spectroscopy (EIS), cyclic voltammetry (CV) and galvanostatic charge–discharge (GCD). The electrochemical behaviors were revealed by three-electrode system in a 0.5 M NaCl solution consisting of 20CTO-PC (working electrode)，a graphite sheet (counter electrode) and a calomel electrode (reference electrode). CV and GCD curves testing were performed in a 0.5 M motionless NaCl solution at the beaker, with the working voltage range from 0 to 1.2 V (vs. RHE). Based on following eqn (S1), the specific capacitance could be calculated.[1, 2]

$$C_i = \frac{Q}{2mv\Delta V} \quad \text{(S1)}$$

Where C_i, Q, m, v and ΔV stand for the electrode specific capacitance, the mathematical integral area of CV curve, the mass of the working electrode, the scan rate and the voltage change, respectively.

In addition, the CV tests of 20CTO-PC at low scan rate (0.5 mV/s and 0.2 mV/s) were carried by three-electrode system in a 500 mg L^{-1} NaCl solution consisting of 20CTO-PC (working electrode)，Pt foil (counter electrode) and a calomel electrode (reference electrode).

The proportion contribution of capacitive-controlled and diffusion-controlled could be calculated by the following eqn (S2):[2, 3]

$$i(\mathrm{v}) = k_1 v + k_2 v^{0.5} \quad \text{(S2)}$$

Where i, v, $k_1 v$ and $k_2 v^{0.5}$ respectively stand for the current, the scanning rate, the capacitive current and the current resulting from diffusion-controlled. Besides, k_1 and k_2 stand for constant under the settled potential.

The CDI performances were assessed by batch mode electrosorption with recycling system, as described in our previous work. The electrodes were prepared by mixing with the samples, acetylene black, and polytetrafluoroethylene preparation (8 : 1 : 1 in weight) to form a slurry. The slurry was laid flat on the graphite sheet and then dried at 120 ℃ about 12 h in order to remove the solvent from the electrode material. In all electrodes, the mass of anode and cathode were the same in each electrode pair. The active material in every electrode was 0.024 g. The total mass of active materials for electrodes is 0.048 g.

Herein, based on the following equation, the salt adsorption capacity (SAC, mg L^{-1})

could be calculated (eqn (S3)):[1, 4-6]

$$\mathrm{SAC} = \frac{(C_o - C_t)\mathrm{V}}{m} \quad \text{(S3)}$$

Where C_0 (mg L^{-1}), C_t (mg L^{-1}), V(L), and m respectively stand for the initial NaCl concentration, the final NaCl concentration, the volume of the NaCl solution and the total mass of the electrodes. The data were obtained by excluding the influence of parasitic electrodes (pure graphite electrodes).

Based on the following eqn (S4), the concentration reduction (CR, mM) could be calculated.[7]

$$\mathrm{CR} = \frac{\mathrm{C_o} - \mathrm{C_t}}{\mathrm{M}} \quad \text{(S4)}$$

Where M stands for sodium chloride mole weight.

Based on the following eqn (S5), the salt adsorption rate (SAR, mg g^{-1} min^{-1}) could be calculated.[1, 8]

$$\mathrm{SAR} = \frac{SAC}{t} \quad \text{(S5)}$$

Where t (min) stands for the desalination time.

The average salt removal rate (ASAR, mg g^{-1} min^{-1}) is the average of all SAR values obtained throughout the desalination period.[4, 9]

Based on the following eqn (S6), for constant-voltage water purification test, the specific energy consumption (SEC^{-1}, mg J^{-1}) could be calculated.[10, 11]

$$SEC^{-1} = \frac{(C_0 - C_t)V}{\mathrm{V_d} \int_0^t I dt} \quad \text{(S6)}$$

Where I (A) and V_d (V) respectively stand for the time dependent current and applied voltage.

Based on the following eqn (S7), the charge efficiency (Λ, %) could be calculated.[9, 12]

$$\Lambda = \frac{\Gamma \times F}{\Sigma} \quad \text{(S7)}$$

Where Γ, F and Σ respectively stand for deionization capacity, Faraday constant and obtained by integrating current.

Based on the following eqn (S8), the water recovery (WR, %) could be calculated.[7, 11]

$$\mathrm{WR} = \frac{\mathrm{V_1 t_1}}{\mathrm{V_1 t_1 + V_2 t_2}} \quad \text{(S8)}$$

Where V_1, t_1, V_2 and t_2 stand for the volume of initial NaCl solution, the time of NaCl removed in one cycle, the volume of recuperative initial NaCl solution and the time of recuperating initial NaCl solution. There is concentration recycle, resulting in V_1=V_2.

Based on the following eqn (S9), the energy consumption (EC, J g^{-1}) could be calculated.[7]

$$\mathrm{EC} = \frac{\mathrm{V_d} \int_0^t I dt}{m} \quad \text{(S9)}$$

Based on the following eqn (S10), the product water-specific Gibbs free energy (△g, J g^{-1}) could be calculated.[13]

$$\triangle \mathrm{g} = 2\mathrm{RT}\left\{\frac{C_0}{WR}\ln\left[\frac{C_0 - C_t WR}{C_0(1-WR)}\right] - C_t \ln\left[\frac{C_0 - C_t WR}{C_t(1-WR)}\right]\right\} \quad \text{(S10)}$$

Where R and T stand for the ideal gas constant and the absolute temperature.

Based on the following eqn (S11), the energy efficiency (EE, %) could be calculated.[13]

$$\mathrm{EE} = \frac{\triangle \mathrm{g}}{EC} \quad \text{(S11)}$$

Based on the following eqn (S12), the Na^+ diffusion coefficient (D_{Na^+}, in cm^2 s^{-1}) could be calculated.[14]

$$\mathrm{D_{Na^+}} = \frac{1}{2}\left(\frac{\mathrm{RT}}{\mathrm{F^2 c \sigma A}}\right)^2 \quad \text{(S12)}$$

where R, T, F, c, σ and A stand for gas constant, temperature, Faraday constant, Na^+

concentration in bulk electrolytes, diffusion resistance obtained by fitting Nyquist plots and electrode geometric area.

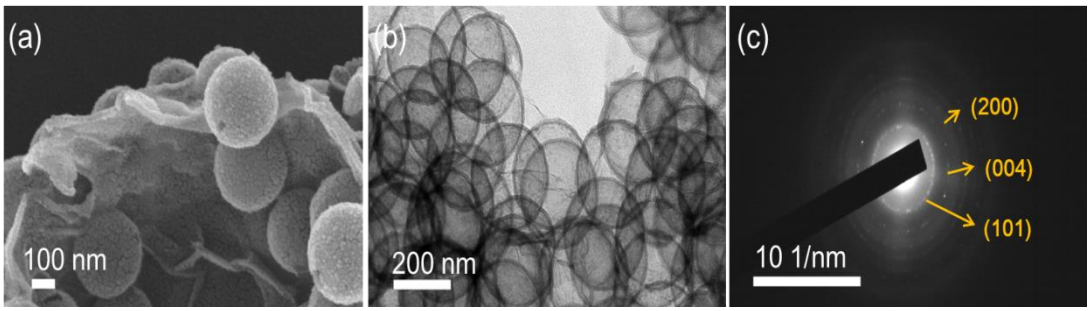

Fig. S1. (a) SEM, (b) TEM, and (c) SAED pattern of 20CTO-PC.

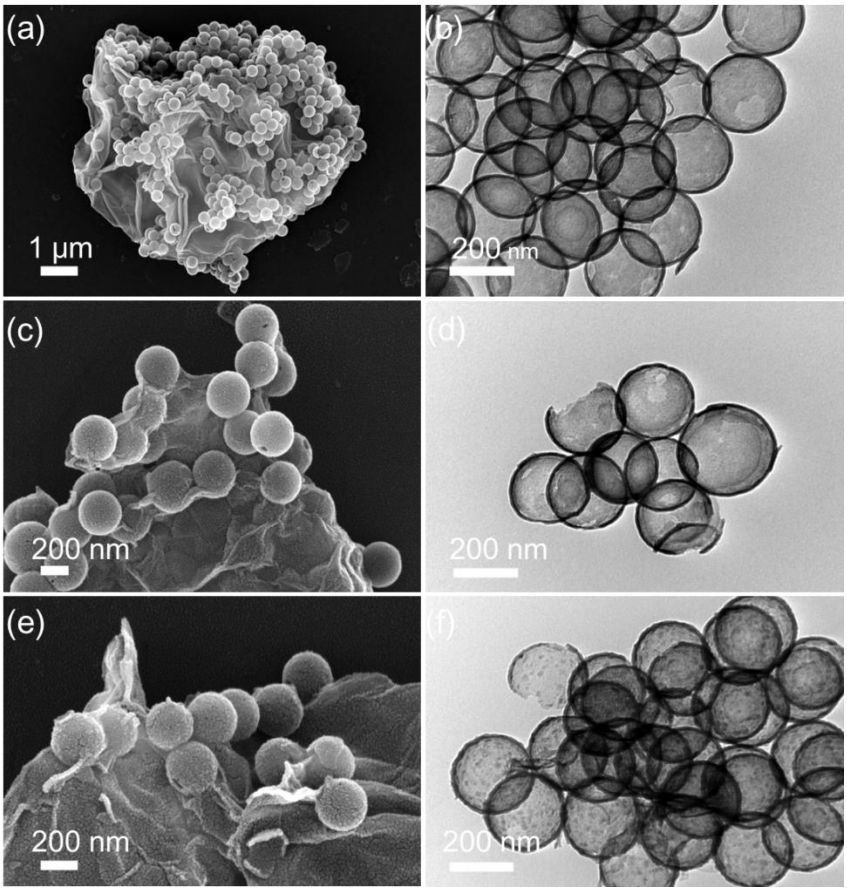

Fig. S2. (a) SEM and (b) TEM images of PC. (c) SEM and (d) TEM images of 10CTO-PC. (e) SEM and (f) TEM images of 30CTO-PC.

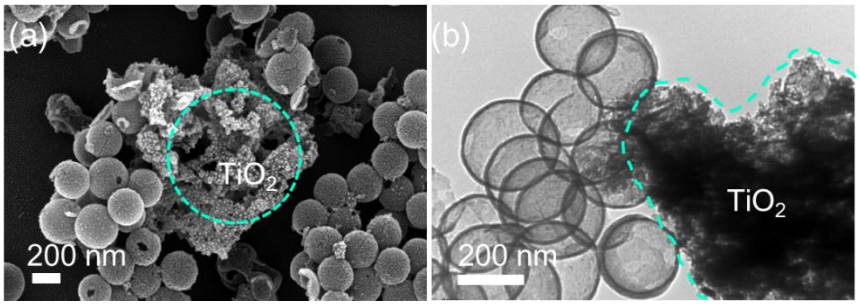

Fig. S3. (a) SEM and (b) TEM images of CTO-PC prepared by an impregnation method.

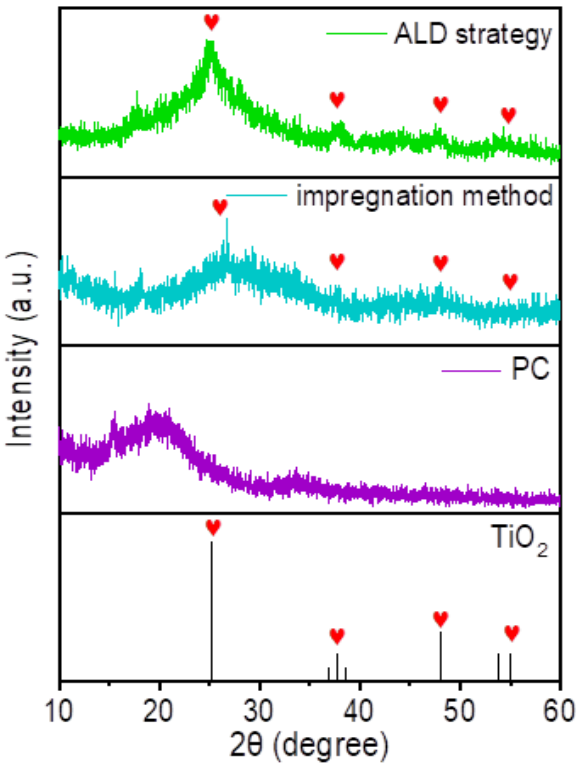

Fig.S4. XRD patterns of CTO-PC prepared by different preparation strategies.

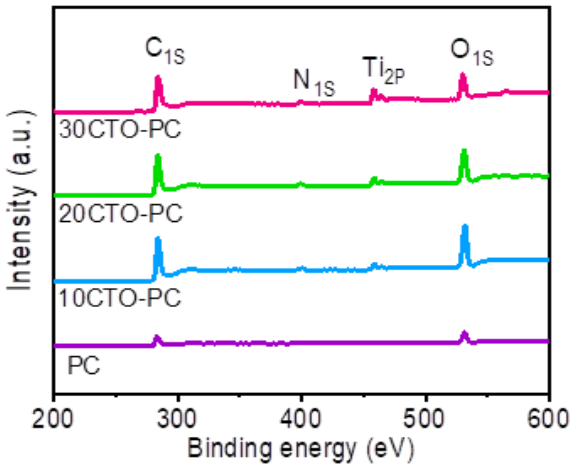

Fig. S5. Full XPS spectra of PC and CTO-PC prepared by an ALD strategy.

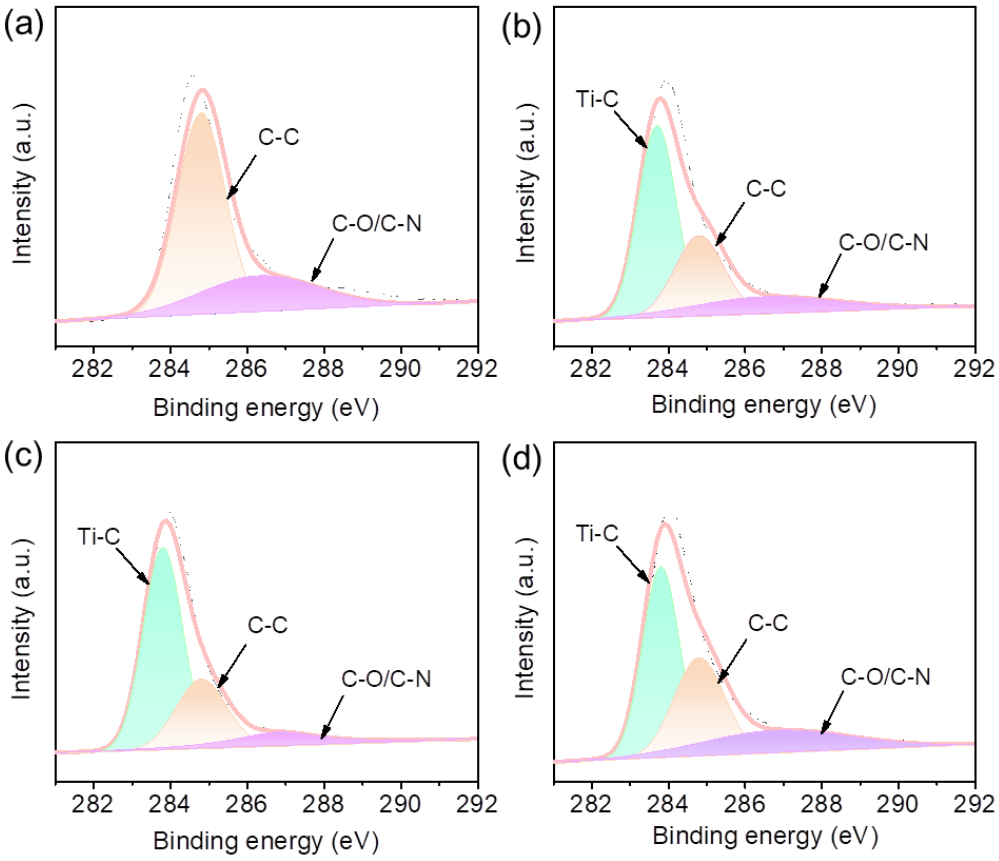

Fig. S6. C_{1s} XPS spectra for (a) PC, (b) 10CTO-PC, (c) 30CTO-PC and (d) CTO-PC prepared by an impregnation method.

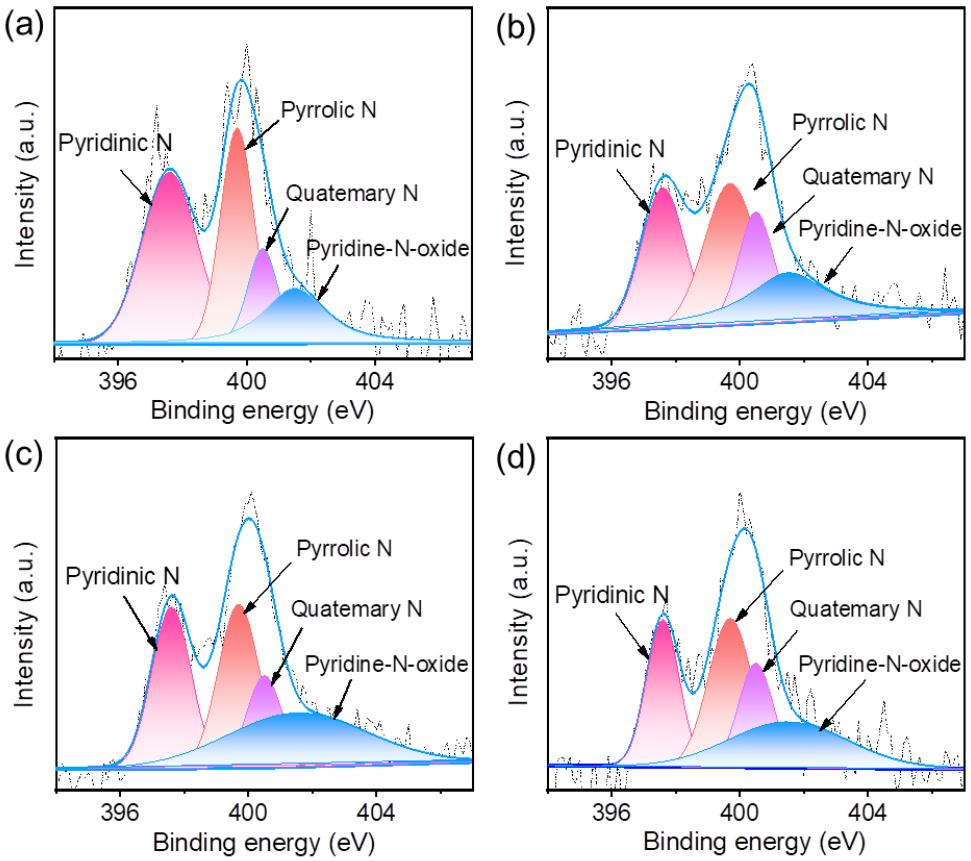

Fig. S7. N_{1s} XPS spectra for (a) PC, (b) 10CTO-PC, (c) 20CTO-PC, and (d) 30CTO-PC.

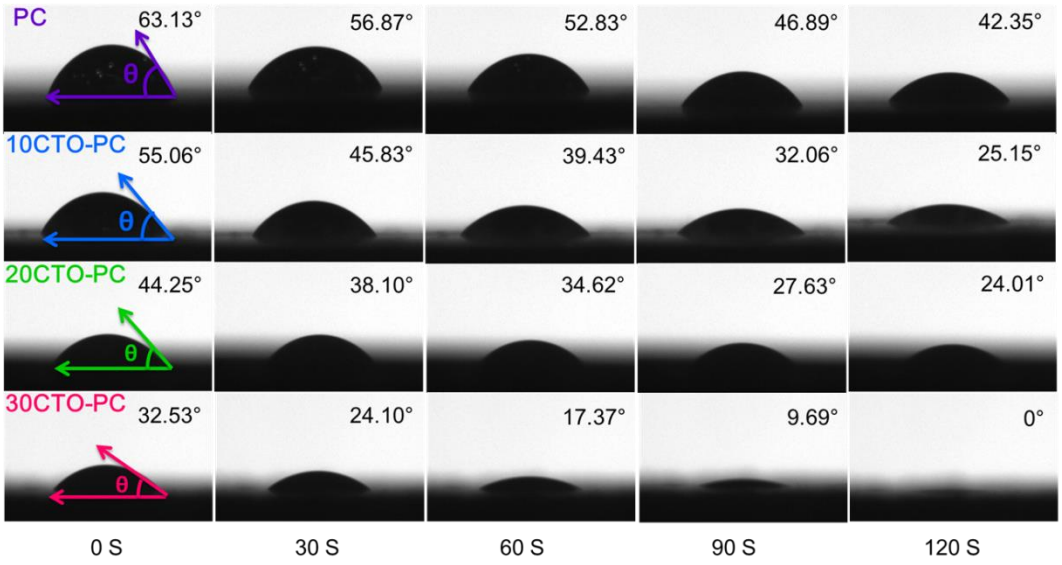

Fig. S8. Optical micrographs of the water contact angles on the surface of PC, 10CTO-PC, 20CTO-PC and 30CTO-PC as a function of contact time.

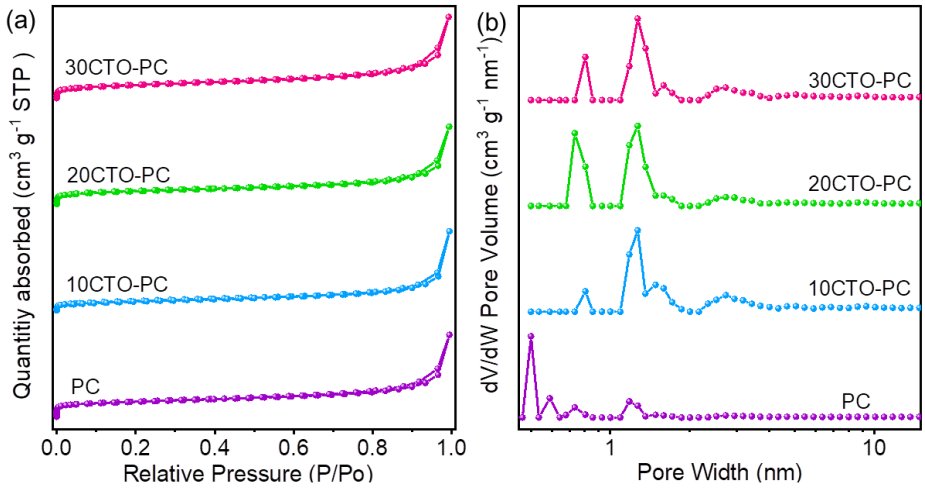

Fig.S9. (a) N_2 adsorption-desorption isotherms and (b) pore size distribution profiles.

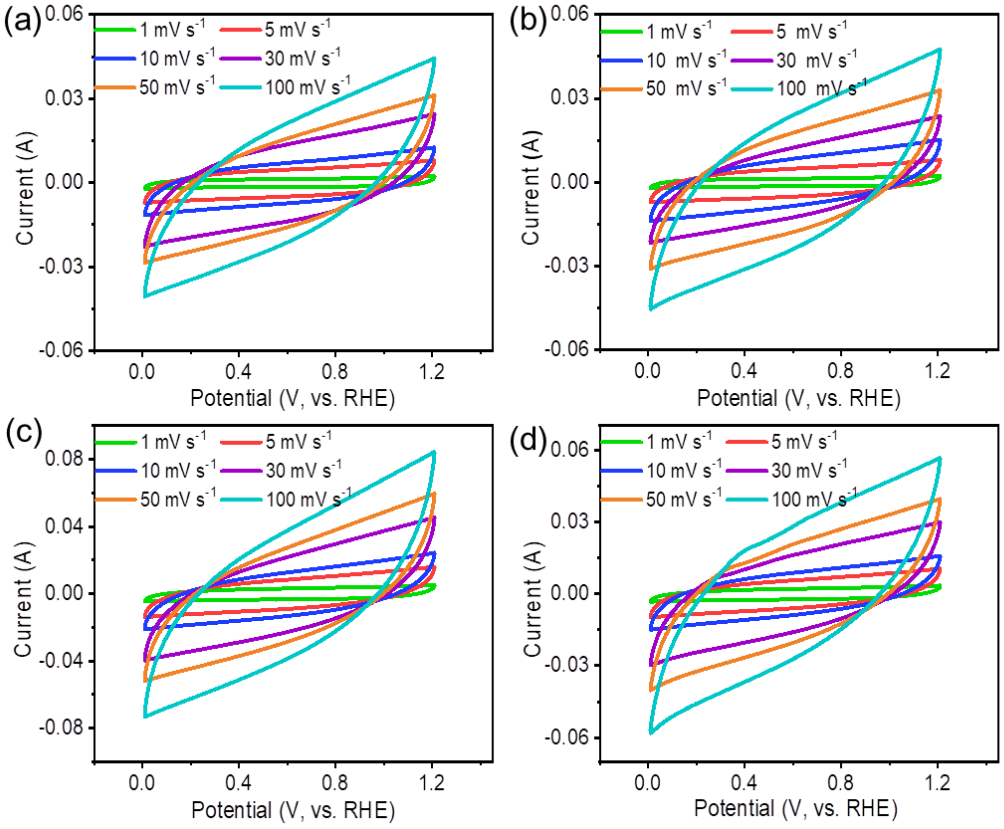

Fig. S10. CV curves in a 0.5 M NaCl solution of (a) PC, (b) 10CTO-PC, (c) 20CTO-PC and (d) 30CTO-PC at scan rates from 1, 5, 10, 30, 50 to 100 mV s^{-1}.

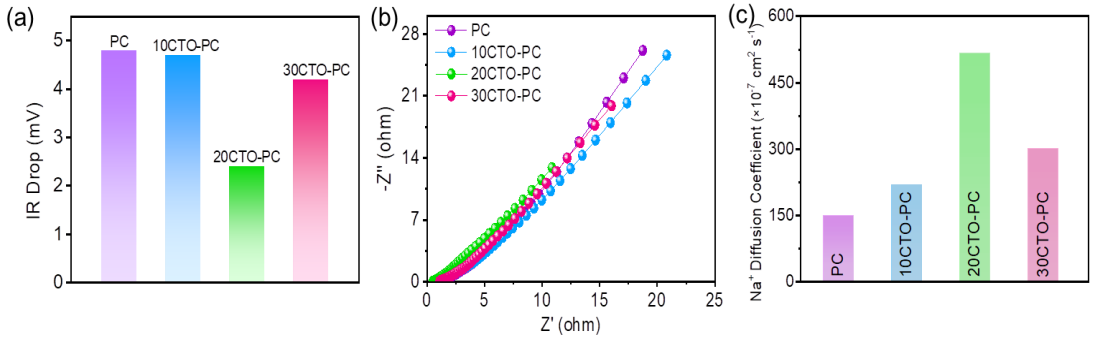

Fig. S11. (a) IR drops of PC, 10CTO-PC, 20CTO-PC and 30CTO-PC. (b) EIS curves of PC, 10CTO-PC, 20CTO-PC and 30CTO-PC. (c) Diffusion coefficients of Na^+ in different samples probed by EIS.

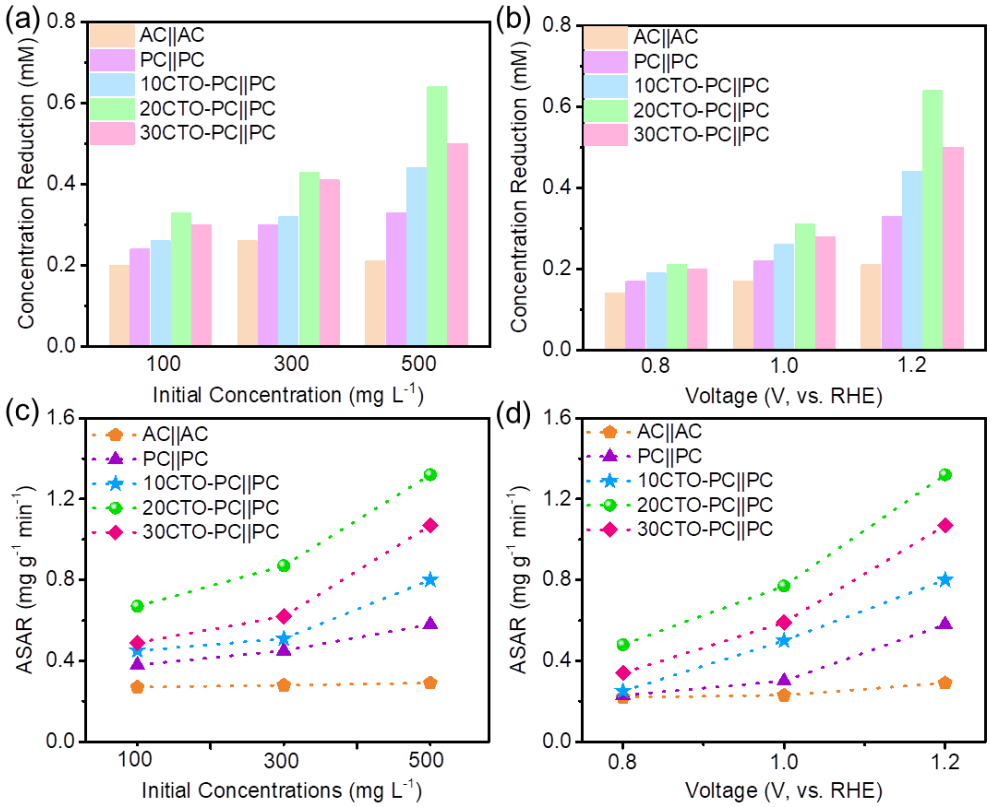

Fig. S12. (a) Plots of concentration reduction vs. different initial concentration for different samples at 1.2 V with a flow rate of 40 mL min^{-1}. (b) Plots of concentration reduction vs. different voltage for different samples in a 500 mg L^{-1} NaCl solution with a flow rate of 40 mL min^{-1}. (c) Plots of ASAR vs. different initial concentration for different samples. (d) Plots of ASAR vs. different voltage for different samples.

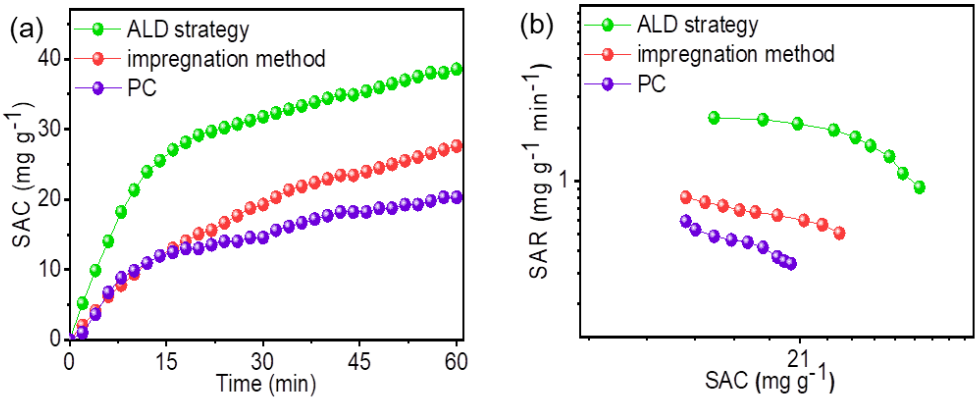

Fig. S13. (a) Plots of SAC vs. deionization time of PC, 20CTO-PC prepared via an ALD strategy and CTO-PC prepared via an impregnation method in a 500 mg L^{-1} NaCl solution at 1.2 V with a flow rate of 40 mL min^{-1}. (b) Ragone plots of PC, 20CTO-PC prepared via an ALD strategy and CTO-PC prepared via an impregnation method.

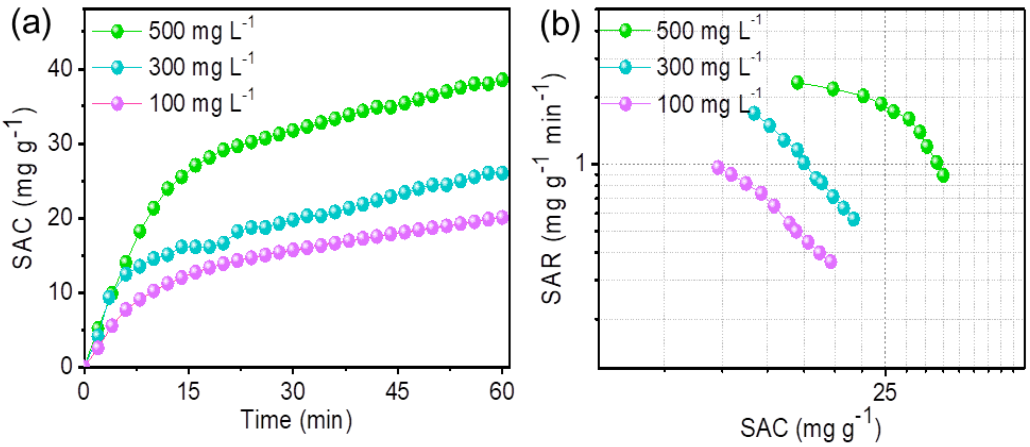

Fig. S14. (a) Plots of SAC vs. deionization time of 20CTO-PC||PC in different initial concentrations of NaCl solution. (b) Ragone plots in different concentrations of NaCl solution.

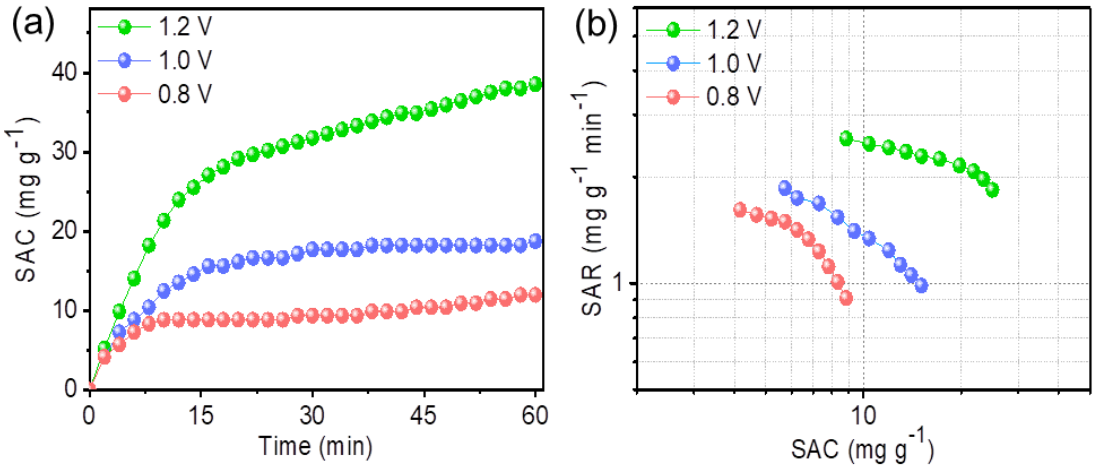

Fig. S15. (a) Plots of SAC vs. deionization time of 20CTO-PC||PC at different voltages. (b) Ragone plots at different voltages.

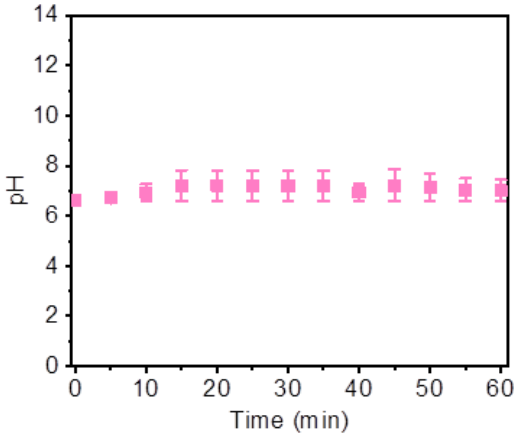

Fig.S16. Plot of pH vs. deionization time of 20CTO-PC||PC in a 500 mg L^{-1} NaCl solution.

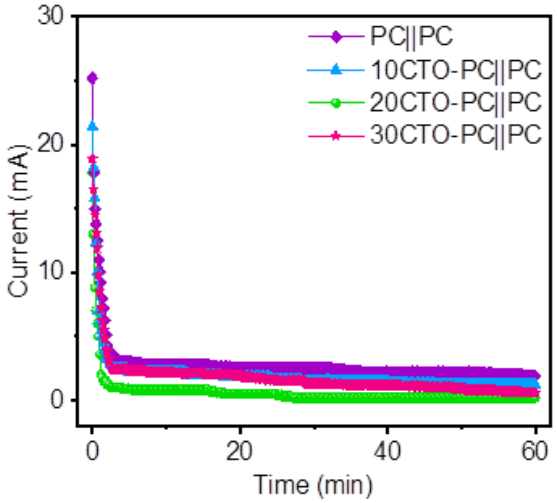

Fig. S17. Current transient curves and time of PC||PC, 10CTO-PC||PC, 20CTO-PC||PC and 30CTO-PC||PC electrodes in a 500 mg L^{-1} NaCl solution at 1.2 V with a flow rate of 40 mL min^{-1}.

Table S1. The content of TiO_2 in different samples.

Sample	TiO_2 (wt%)
10CTO-PC	3.53
20CTO-PC	6.95
30CTO-PC	10.97
CTO-PC prepared by impregnation	7.10

Table S2. Elemental composition of C, O, N and Ti in different samples.

Sample	C (at%)	O (at%)	N (at%)	Ti (at%)
PC	58.39	38.00	3.61	0
10CTO-PC	64.14	31.89	3.37	0.60
20CTO-PC	65.49	28.53	4.79	1.19
30CTO-PC	73.28	20.16	4.69	1.87
CTO-PC prepared by impregnation	71.39	22.96	4.45	1.20

Table S3. Comparative results on the removal capacity among different materials.

Materials	voltage (V)	NaCl concentration (mg L^{-1})	Removal capacity (mg g^{-1})	References
N-doped carbon sphere	1.2	500	13.71	[15]
3D porous graphene	1.4	300	18.43	[16]
graphene aerogel/TiO_2	1.2	500	15.1	[17]
HC@MnO_2	1.2	500	30.7	[6]
TiO_2-NTs/C	1.2	500	13.11	[18]
Graphene/Co_3O_4	1.6	500	20.16	[19]
MoS_2−graphene	1.2	500	19.4	[2]
ZnO/AC	1.2	500	9.4	[20]
NaOH-$Ti_3C_2T_x$	1.2	500	16.02	[21]
MoS_2/g-C_3N_4	1.6	250	24..2	[22]
$Ti_3C_2T_x$–MXene	1.2	500	26.7	[23]
3DOM-TiN	1.2	500	23.6	[24]
20CTO-PC	1.2	500	38.54	This work

■ REFERENCES

1. G. Wang, T. Yan, J. Zhang, L. Shi and D. Zhang, Trace-Fe-Enhanced Capacitive Deionization of Saline Water by Boosting Electron Transfer of Electro-Adsorption Sites, *Environ. Sci. Technol.*, 2020, **54**, 8411-8419.
2. J. Han, T. Yan, J. Shen, L. Shi, J. Zhang and D. Zhang, Capacitive Deionization of Saline Water by Using MoS_2-Graphene Hybrid Electrodes with High Volumetric Adsorption Capacity, *Environ. Sci. Technol.* , 2019, **53**, 12668-12676.
3. N. Wang, X. Xu, T. Liao, Y. Du, Z. Bai and S. Dou, Boosting Sodium Storage of Double-Shell Sodium Titanate Microspheres Constructed from 2D Ultrathin Nanosheets via Sulfur Doping, *Adv. Mater.*, 2018, **30**, 1804157.
4. T. Liu, J. Serrano, J. Elliott, X. Yang, W. Cathcart, Z. Wang, Z. He and G. Liu, Exceptional capacitive deionization rate and capacity by block copolymer–based porous carbon fibers, *Sci. Adv.*, 2020, **6**, eaaz0906.
5. J. Ma, Y. Xiong, X. Dai and F. Yu, Zinc Spinel Ferrite Nanoparticles as a Pseudocapacitive Electrode with Ultrahigh Desalination Capacity and Long-Term Stability, *Environ. Sci. Technol. Lett.*, 2020, **7**, 118-125.
6. S. Wang, G. Wang, T. Wu, C. Li, Y. Wang, X. Pan, F. Zhan, Y. Zhang, S. Wang and J. Qiu, Membrane-Free Hybrid Capacitive Deionization System Based on Redox Reaction for High-Efficiency NaCl Removal, *Environ. Sci. Technol.*, 2019, **53**, 6292-6301.
7. S. A. Hawks, A. Ramachandran, S. Porada, P. G. Campbell, M. E. Suss, P. M.

Biesheuvel, J. G. Santiago and M. Stadermann, Performance metrics for the objective assessment of capacitive deionization systems, *Water Res.*, 2019, **152**, 126-137.

8. J. Zhang, T. Yan, J. Fang, J. Shen, L. Shi and D. Zhang, Enhanced capacitive deionization of saline water using N-doped rod-like porous carbon derived from dual-ligand metal-organic frameworks, *Environ. Sci.: Nano*, 2020, **7**, 926-937.

9. G. Tan, S. Lu, N. Xu, D. Gao and X. Zhu, Pseudocapacitive Behaviors of Polypyrrole Grafted Activated Carbon and MnO_2 Electrodes to Enable Fast and Efficient Membrane-Free Capacitive Deionization, *Environ. Sci. Technol.*, 2020, **54**, 5843-5852.

10. L. Wang and S. Lin, Intrinsic tradeoff between kinetic and energetic efficiencies in membrane capacitive deionization, *Water Res.*, 2018, **129**, 394-401.

11. S. K. Patel, M. Qin, W. S. Walker and M. Elimelech, Energy Efficiency of Electro-Driven Brackish Water Desalination: Electrodialysis Significantly Outperforms Membrane Capacitive Deionization, *Environ. Sci. Technol.*, 2020, **54**, 3663-3677.

12. H. Zhang, W. Zhang, J. Shen, Y. Li, X. Yan, J. Qi, X. Sun, J. Shen, W. Han, L. Wang and J. Li, Ag-doped hollow ZIFs-derived nanoporous carbon for efficient hybrid capacitive deionization, *Desalination*, 2020, **473**, 114173.

13. S. Lin, Energy Efficiency of Desalination: Fundamental Insights from Intuitive

Interpretation, *Environ. Sci. Technol.*, 2020, **54**, 76-84.

14. T. Liu, J. Serrano, J. Elliott, X. Yang, W. Cathcart, Z. Wang, Z. He and G. Liu, Exceptional capacitive deionization rate and capacity by block copolymer–based porous carbon fibers, *Sci. Adv.*, 2020, **6**, :eaaz0906.

15. Y. Liu, T. Chen, T. Lu, Z. Sun, D. H. C. Chua and L. Pan, Nitrogen-doped porous carbon spheres for highly efficient capacitive deionization, *Electrochim. Acta*, 2015, **158**, 403-409.

16. A. G. El-Deen, R. M. Boom, H. Y. Kim, H. Duan, M. B. Chan-Park and J. H. Choi, Flexible 3D Nanoporous Graphene for Desalination and Bio-decontamination of Brackish Water via Asymmetric Capacitive Deionization, *ACS Appl. Mater. Interfaces*, 2016, **8**, 25313-25325.

17. H. Yin, S. Zhao, J. Wan, H. Tang, L. Chang, L. He, H. Zhao, Y. Gao and Z. Tang, Three-dimensional graphene/metal oxide nanoparticle hybrids for high-performance capacitive deionization of saline water, *Adv. Mater.*, 2013, **25**, 6270-6276.

18. K. Wei, Y. Zhang, W. Han, J. Li, X. Sun, J. Shen and L. Wang, A novel capacitive electrode based on TiO_2-NTs array with carbon embedded for water deionization: Fabrication, characterization and application study, *Desalination*, 2017, **420**, 70-78.

19. G. Divyapriya, K. K. Vijayakumar and I. Nambi, Development of a novel graphene/Co_3O_4 composite for hybrid capacitive deionization system, *Desalination*, 2019, **451**, 102-110.

20. J. Liu, M. Lu, J. Yang, J. Cheng and W. Cai, Capacitive desalination of ZnO/activated carbon asymmetric capacitor and mechanism analysis, *Electrochim. Acta*, 2015, **151**, 312-318.

21. B. Chen, A. Feng, R. Deng, K. Liu, Y. Yu and L. Song, MXene as a Cation-Selective Cathode Material for Asymmetric Capacitive Deionization, *ACS Appl. Mater. Interfaces*, 2020, **12**, 13750-13758.

22. S. Tian, X. Zhang and Z. Zhang, Capacitive deionization with MoS_2/g-C_3N_4 electrodes, *Desalination*, 2020, **479**, 114348.

23. W. Bao, X. Tang, X. Guo, S. Choi, C. Wang, Y. Gogotsi and G. Wang, Porous Cryo-Dried MXene for Efficient Capacitive Deionization, *Joule*, 2018, **2**, 778-787.

24. Y. Wu, G. Jiang, G. Liu, G. Lui, Z. P. Cano, Q. Li, Z. Zhang, A. Yu, Z. Zhang and Z. Chen, A 3D ordered hierarchically porous non-carbon electrode for highly effective and efficient capacitive deionization, *J. Mater.Chem. A*, 2019, **7**, 15633-15639.